Hole selective materials and device structures of heterojunction solar cells: Recent assessment and future trends

Cite as: APL Mater. 7, 110701 (2019); doi: 10.1063/1.5121327
Submitted: 9 August 2019 • Accepted: 24 October 2019 •
Published Online: 8 November 2019

Zilei Wang,[1,2] Peiyang Li,[1] Zhaolang Liu,[1] Jiandong Fan,[1] Xiaokang Qian,[1] Jian He,[3] Shanglong Peng,[2] Deyan He,[2] Meicheng Li,[4] and Pingqi Gao[1,a)]

AFFILIATIONS

[1]School of Materials, Sun Yat-Sen University, Guangzhou 510275, China
[2]School of Physical Science and Technology, Lanzhou University, Lanzhou 730000, China
[3]Research School of Engineering, The Australian National University, Canberra, ACT 2602, Australia
[4]State Key Laboratory of Alternate Electrical Power System with Renewable Energy Sources, North China Electric Power University, Beijing 102206, China

[a)]Author to whom correspondence should be addressed: gaopq3@mail.sysu.edu.cn

ABSTRACT

Research on photovoltaic devices with a high performance-to-cost ratio requires efforts not only on efficiency improvement but also on manufacturing cost reduction. Recently, a record efficiency of 26.6% on crystalline silicon solar cells (SCs) has been achieved by combining the heterojunctions (HJs) with a device structure of interdigitated back contacts. However, the technology that integrates the interdigital *p*- and *n*-type amorphous silicon (a-Si:H) layers on the rear surface of the Si substrate is challenging. This issue has motivated researchers to search dopant-free carrier-selective contacts with alternative materials to completely replace doped a-Si:H layers. Transition metal oxides, graphene, and poly(3,4-ethylene dioxythiophene):poly(styrenesulfonate) (PEDOT:PSS), all having high work functions and hole conducting properties, can play the role of hole-selective layers (HSLs). In this review, we focus on the latest advances and the future trends in these HSLs and their applications in silicon HJ SCs. The main issues and challenges encountered are discussed.

I. INTRODUCTION

As a promising alternative technique to crystalline silicon (c-Si) solar cells (SCs) for a higher performance-to-cost ratio, passivation contacts [also known as heterocontacts or carrier selective contacts (CSCs)] attract ever-increasing interest. An ideal passivation contact can suppress the electrical losses at interfaces to the utmost by maintaining an ultralow contact resistivity for transportation of only one type of carriers (holes or electrons) while maintaining a larger barrier for the other type (see Fig. 1). For example, the TiO_x layer is often used as an electron selective contact due to a very small conduction band offset (about 0.05 eV) and a large valence band offset (>2.0 eV) at the n-Si/TiO_x interface.[1] Recently, c-Si solar cells with a record efficiency of 24.4% (module, double-sided junctions)[2] and 26.6% [laboratorial, interdigitated back contact (IBC) structure][3] have been achieved, largely owing to the application of passivation contacts. In these two types of devices, intrinsic hydrogenated amorphous silicon [a-Si:H(i)] was used to passivate the Si surface and *p*/*n*-type doped hydrogenated amorphous silicon [a-Si:H(p)/a-Si:H(n)] was employed to deliver carrier-selective transport. However, such solar cells still suffer from unnecessary optical/electrical losses because of the parasitic absorption/Auger recombination inherent to the doped a-Si:H films. These issues have motivated researchers to search alternative materials to completely replace doped a-Si:H layers, which usually are called dopant-free carrier-selective contacts (CSCs). When the dopant-free CSCs are deposited on both sides of c-Si wafers, these novel devices are nominated as dopant-free asymmetric heterocontact (DASH)

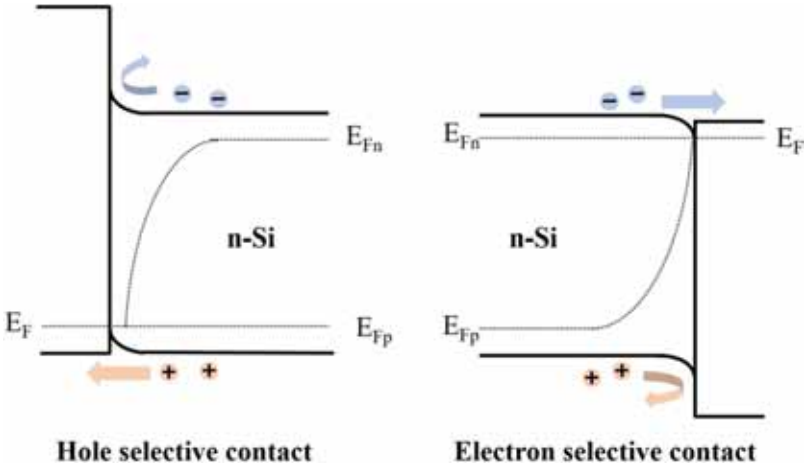

FIG. 1. Schematic band diagrams for examples of ideal hole/electron selective contact concepts on *n*-type c-Si.

solar cells.[4,5] The functional materials involved in these kinds of devices can always be more easily deposited via spin-coating or thermal evaporation, and the performance-to-cost ratio will be further boosted by cutting the material cost to the bone.

From a band alignment view, transition metal oxides (TMOs: MoO_x, V_2O_x, WO_x, etc.),[6–9] poly(3,4-ethylene dioxythiophene): poly(styrenesulfonate) (PEDOT:PSS),[10,11] and graphene,[12,13] all having high work functions (WFs) and hole conducting properties, can play the role of hole-selective layers (HSLs). Connecting HSLs with c-Si, the Fermi levels of these two materials will be aligned. This will result in a large conduction band offset on the Si surface, leading to a strong inversion layer with accumulation of holes. The heterojunction (HJ) works more like a p-n junction and produces a high enough built-in potential. Promising efficiencies of 20.7%[4] and 22.5%,[14] for the solar cells featuring either full- or half-dopant-free heterocontacts, have been reported recently.

In this review, we first discuss the design and production of silicon heterojunction (SHJ) solar cells. We then discuss TMOs and TMO/Si heterojunction solar cells (HSCs). Finally, other types of HSLs will also be addressed. Attention will be emphasized on the latest advances in the modification of HSL materials, interfacial passivation, contact resistivity, and device structures.

II. SILICON HETEROJUNCTION (SHJ) SOLAR CELL

A. Overview of the SHJ solar cell

The silicon heterojunction (SHJ) solar cell was first developed by Sanyo Corporation in early 1990s, which was called the HIT (heterojunction with an intrinsic thin layer) structure.[15,16] The SHJ structure is one of the most cutting edge structures of the c-Si solar cell until now because the highest efficiency (26.6%) has been reached by combining the SHJs with the device structure of interdigitated back contacts (IBCs).[3] The key factor of the SHJ device structure is the introduction of an a-Si:H(i) layer with a thickness of several nanometers,[17,18] which can compensate the dangling bonds existing at the interface of the c-Si wafer. An ultrahigh minority carrier lifetime is thus obtained. Moreover, electron- and hole-selective contacts are achieved by sandwiching the c-Si wafer with a-Si:H(i)/a-Si:H(n) and a-Si:H(i)/a-Si:H(p) stacks, respectively. The complete structure of the SHJ solar cell is shown in Fig. 2(a).[19]

Traditional silicon solar cells introduce dielectric layers and a passivated emitter and rear cell (PERC) (PERL and PERT) to acquire the passivation effect, as shown in Fig. 2(b). However, the recombination at the interface of metal/Si is still a severe issue, causing limitations on the cell efficiencies. Furthermore, these configurations lead to an increase of the processing steps, making this manufacturing process less attractive. SHJ solar cells are currently one of the most successful passivation contact structures with following advantages. First, a-Si:H enables excellent chemical passivation on the Si absorber. Second, a significant inversion effect existed at the a-Si:H/c-Si interface that can further promote the carrier lifetime by field-effect passivation. Furthermore, from the processing perspective, few process steps are required to complete a solar device, and the low-temperature (<200 °C) processing enables the use of very thin wafers without causing substrate warping. The full processing sequence is given in Fig. 2(c).

B. Current achievements of SHJ

By routinely optimizing the a-Si:H(i) passivation layer, the front contact [highly conductive transparent conductive oxide (TCO) and metal grid lines], and the back contact (passivation and contact resistivity), Panasonic has achieved cell efficiency up to 24.7% for their SHJ solar cells.[20] Kaneka Corporation reported a record-breaking efficiency of 25.1% for SHJ solar cells in 2015.[21] Furthermore, efficiency beyond 24% of SHJ modules has also been reported.[2] The IBC-SHJ solar cell,[22,23] combined with the merits of SHJ and IBC structures, is considered as the most promising structure to approach the theoretical efficiency limit of a c-Si solar cell.[24–28] Based on this structure, Panasonic Corporation achieved a high efficiency of 25.6% (V_{oc} = 740 mV, J_{sc} = 41.8 mA/cm^2, FF = 82.7%, 143.7 cm^2). Kaneka Corporation reported an efficiency of 26.3%[29] and then a record-breaking efficiency of 26.6% (V_{oc} = 740 mV, J_{sc} = 42.5 mA/cm^2, FF = 84.6%, 179.7 cm^2).[3]

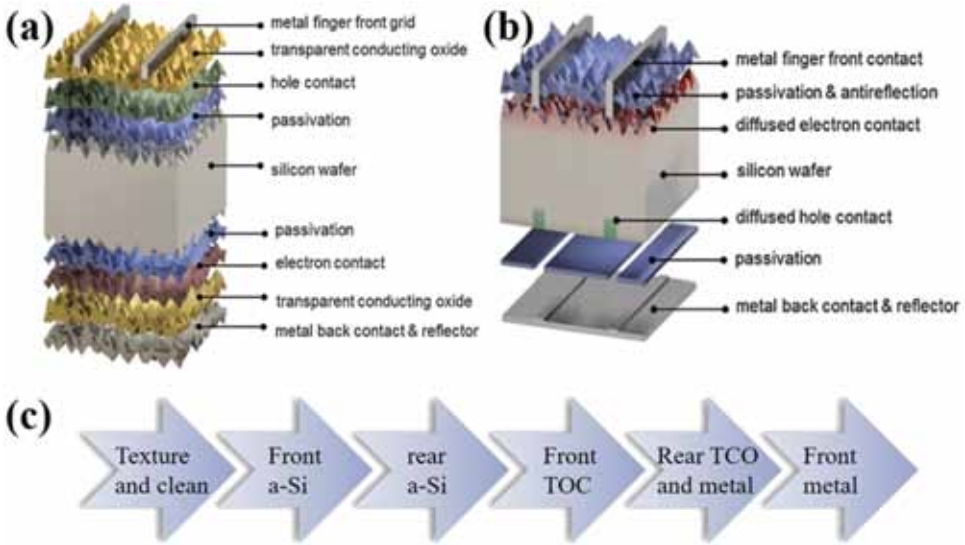

FIG. 2. Schematic of the components of the (a) silicon heterojunction cell and (b) localized rear contact solar cell with dielectric rear surface passivation. Reprinted with permission from Battaglia *et al.*, Energy Environ. Sci. **9**, 1552 (2016). Copyright 2016 Royal Society of Chemistry. (c) The full device processing sequence of SHJ solar cells.

C. Bottlenecks in energy production and efficiency

1. Optical losses due to parasitic absorption

Despite the significant achievements, the a-Si:H layers in SHJ cells will result into apparently parasitic light absorption, causing unsatisfied J_{sc}. Figure 3(a) shows a noticeable absorption spectrum of the a-Si:H layer at short wavelength from 300 to 600 nm.[30] This corresponds to a J_{sc} loss of 2.1 mA/cm^2 [see Fig. 3(b)].[31] Moreover, because of the poor conductivity of the a-Si:H(i) film, one has to deposit a transparent conductive oxide (TCO) film upon it to effectively collect photogenerated carriers and laterally transport them to the front electrode grid. Undesirably, as shown in Fig. 3(b), the TCO films absorb the IR light due to strong excitation of free carriers, leading to J_{sc} loss at long wavelength.

2. Electrical losses due to Auger recombination

Auger recombination will become the predominant factor in SHJ solar cells in the premise of good interface passivation and high-quality Si wafers. Auger recombination is a two-particle process that has a complex dependence on the carrier concentrations. Figure 4 shows the recombination current density at the maximum power point ($J_{rec\text{-}mpp}$), which is divided by the contributions of the different recombination mechanisms. $J_{rec\text{-}mpp}$ was calculated as a function

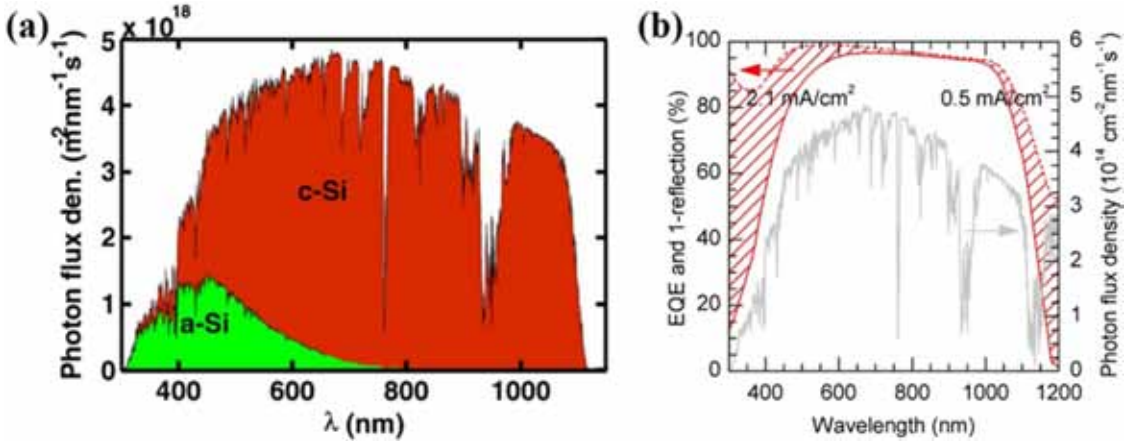

FIG. 3. (a) The photon flux density in the AM1.5G spectrum absorbed in a-Si:H regions at the front and the c-Si absorber. Reprinted with permission from Chavali *et al.*, Prog. Photovoltaics: Res. Appl. **26**, 241 (2016). Copyright 2016 Wiley (b) EQE (red, solid) and 1-reflection (red, dashed) of a high-J_{sc} silicon heterojunction solar cell. The shaded area indicates parasitic absorption, and the associated current density losses below 600 nm and above 1000 nm are given, assuming an AM 1.5G spectrum (gray). Reprinted with permission from Holman *et al.*, IEEE J. Photovoltaics **2**, 7 (2012). Copyright 2012 IEEE.

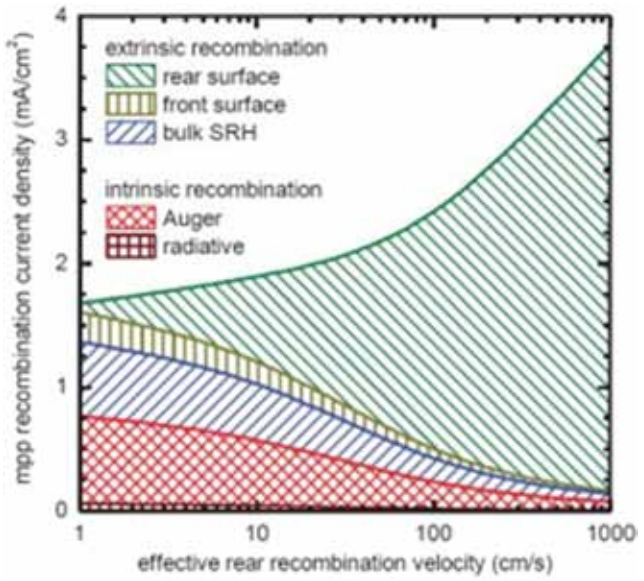

FIG. 4. Recombination current density at the maximum power point ($J_{rec\text{-}mpp}$) as a function of the effective rear recombination velocity. $J_{rec\text{-}mpp}$ is separated into the contribution of each recombination mechanism. The data were simulated using PC1D for an *n*-type silicon solar cell with a 150 μm thick, 1 Ω cm *n*-type silicon base and a shallow industrial boron-doped front side emitter. Reprinted with permission from Richter *et al.*, Energy Procedia **27**, 88 (2012). Copyright 2012 Elsevier.

of the effective rear surface recombination velocity ($S_{eff\text{-}rear}$). It can be seen that with decreasing $S_{eff\text{-}rear}$, the contribution of the Auger recombination increases significantly, reaching about 30% of the total $J_{rec\text{-}mpp}$ at $S_{eff\text{-}rear}$ = 10 cm/s.[32] Therefore, limiting Auger recombination is gaining importance for efficiency improvement of SHJ solar cells.

III. EMERGING TRENDS—TMO/SI HSCs

A. Overview of TMO materials

Transition-metal-oxides (TMOs) are of great interests since they are cost-effective, nontoxic, and easily acquirable. TMOs usually possess wide optical bandgaps (Eg > 3 eV) and wide range variable work functions from 3 to 7 eV. These unique properties make them highly flexible when used as dopant-free carrier-selective contacts.[1,5,7,9,33–38] In addition, these films can be deposited at low temperatures (T < 200 °C) by thermal evaporation or solution-processing methods,[39–41] indicating a great potential for process simplification and cost reduction. The DASH solar cells mentioned above,[4,6–8,42–47] which fully explore the advantages of TMOs, could be one promising alternative for further improving the performance of the state-of-the-art c-Si solar cells.

B. Hole-selective transport

1. Mechanism of hole collection and transport

For TMO/n-Si heterojunction, carrier selectivity is controlled by the band bending induced by TMOs. Most of the TMO materials as hole-selective contacts exhibit work function higher than 5 eV. When these TMOs are connected with *n*-type Si, the Fermi levels' alignment will result into an energy band bending of about 0.8 eV. This leads to a strong inversion layer with an accumulation of holes. This behavior forms the foundation for the high efficiency of TMO/c-Si solar cells. Battaglia considered that the MoOx in MoOx/c-Si cells behave more like a high-work function metal. Band bending occurs on both the c-Si surface and the MoO_x.[14,48] Through investigations with ultraviolet photoelectron spectroscopy (UPS) and x-ray photoelectron spectroscopy (XPS), Sun *et al.* studied the band alignment of MoOx/n-Si and found the existence of an interfacial dipole of ~0.97 eV (corresponding to an energy band bending of ~0.80 eV).[49] A schematic diagram of the energy band of the TMO/a-Si:H(i)/n-Si interface is shown in Fig. 5.

Vijayan[50] and Messmer[51,52] studied the hole transport paths at the TMO/a-Si:H(i)/n-Si interface by simulations. Figure 6 shows the band diagram of the simulated TMO-based silicon heterojunction in the dark at equilibrium. There are two possible transport paths highlighted in the contact, i.e., band-to-band (B2B) tunneling where charge carriers tunnel directly and trap-assisted-tunneling (TAT) where charge carriers tunnel via trap states within the bandgap of the TMO. B2B will be the main transport mode if TMO has a sufficiently high work function, which makes the conduction band of TMO lower than the valence band of n-Si. However, in the condition of TMO with an inadequate work function, the TAT mechanism is necessary and additional series resistance will be introduced.

2. Work function and conductivity

As described in Sec. III B 1, the barrier at the TMO/n-Si interface is controlled by the work function of the TMO. TAT is necessary if the work function of TMO is low. In this condition, the conductivity of TMO becomes a determining parameter for hole transport,

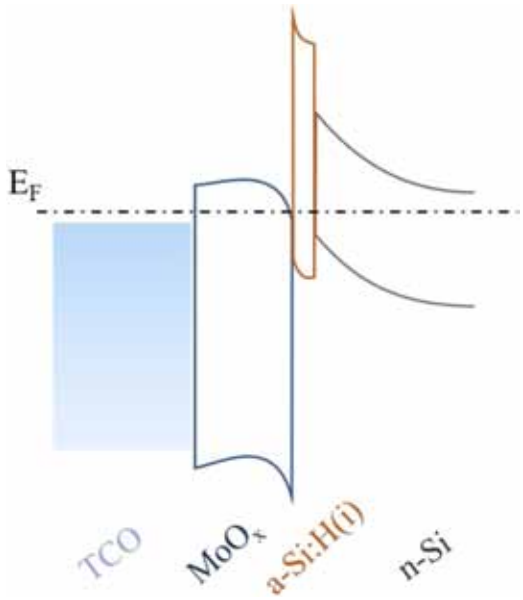

FIG. 5. Schematic diagrams of the energy band for the TMO/a-Si:H(i)/n-Si interface.

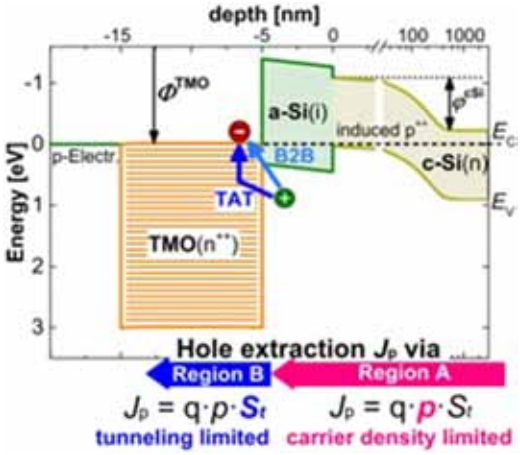

FIG. 6. Schematic diagram of the band structures of the heterojunction between c-Si and transition metal oxides (TMO), with different electron affinities. Reprinted with permission from Messmer *et al.*, J. Appl. Phys. **124**(8), 085702 (2018). Copyright 2018 AIP Publishing LLC.

as shown in Figs. 7(a)–7(c). If the work function further decreases, and the trap states in the TMO are insufficient (i.e., conductivity is unsatisfied), the *J-V* curve will behave as the S-shape and exhibit a low V_{oc}. It is notable that only the low work function alone does not necessarily have an s-shape *J-V* curve. When the work function of TMO is low but the conductivity is sufficiently high, a limitation of the TMO work function alone (while other influences such as the TAT transport stay ideal) theoretically still yields a single diode behavior and therefore no s-shape [see Figs. 7(a)–7(d), red]. This is expected from the following equation:

$$J(V) = J_{s1}\exp\left[-\frac{q\varnothing_B}{kT}\right]\left(\exp\left[\frac{qV}{kT}\right]-1\right) = J_{s1}\left(\exp\left[\frac{qV}{kT}\right]-1\right). \quad (1)$$

However, the hole transport mechanism will conform to band-to-band (B2B) tunneling when the work function is sufficiently high. Figure 7(d) shows the case for a TMO work function of 5.7 eV which implies that the TMO conduction band energy is greater than the n-Si valence band energy and therefore allows for efficient band-to-band tunneling. Thus, the transport is independent of the trap densities (i.e., conductivity), and all *J-V* curves match each other even for the case with very low trap densities. This work together with other similar simulation studies is in qualitative agreement with experiments.[50–53] These results further indicate that the high work function (electron affinity) of TMO is critical to improving the performance of TMO/Si solar cells.

The work function controls the barrier height at the TMO/n-Si interface, while the transfer of holes across the barrier is assisted by the gap defect states. However, the conductivity and work function vary with the oxygen content in an opposite manner. The gap states are mainly originated from the oxygen vacancies, while the work function decreases from the insulators (MoO_3) to the semiconductors (MoO_{3-x}) and then to the metal-like conductors (MoO_2) as the cation oxidation state decreases.[9] State densities of oxygen vacancies are influenced by the substrates, fabrication methods, postdeposition treatments, etc.[54–56] Thermal evaporation is always used to fabricate TMOs. The resulting films are of slightly substoichiometric materials (such as MoO_x, $x < 3$) with an initial work function of around 5.5 eV for the as-deposited sample and then below 5.2 eV after thermal annealing at 180 °C.[57] Besides, the atomic layer deposition (ALD) method,[58,59] solution method,[39–41] chemical vapor deposition (CVD) method,[60,61] and sputtered method[62] were also used to deposit MoO_x thin films with similar work functions.

Figure 8 shows a plot of work function vs O-deficiency. The work function of MoO_x decreases rapidly at the initial stage and then gently decreases with a nearly linear trend. Greiner *et al.*[55] explained this behavior by the following equation:

$$\varnothing = \varnothing_0 + \Delta\varnothing_d + \Delta\varnothing_x, \quad (2)$$

where Ø is the measured work function, $\varnothing_0$ is the work function of the stoichiometric oxide (i.e., MoO_3), $\Delta\varnothing_x$ is the change in work

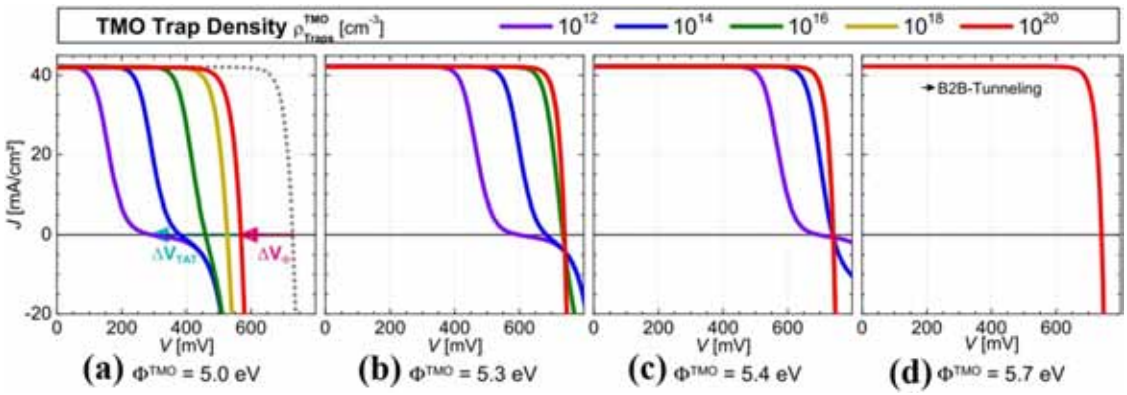

FIG. 7. *J-V* light curves at one sun for different trap densities (colors) and TMO work functions Φ. (a) Φ = 5.0 eV highlights the selectivity losses $\Delta V_{\varnothing}$ due to insufficient Φ and $\Delta V_{\varnothing}$ due to insufficient TAT transport. (b) Φ = 5.3 eV and (c) Φ = 5.4 eV are in the transition region, whereas in (d) Φ = 5.7 eV, band-to-band tunneling dominates. Reprinted with permission from Messmer *et al.*, J. Appl. Phys. **124**(8), 085702 (2018). Copyright 2018 AIP Publishing LLC.

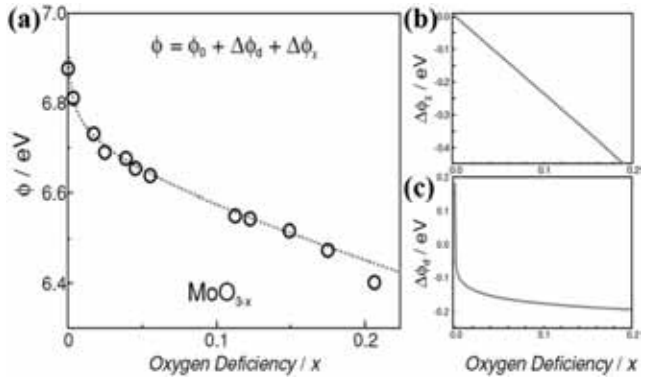

FIG. 8. (a) Work function, (b) electronegativity contribution, and (c) donor state contribution of MoO_x vs oxygen deficiency/x. The circles in (a) are the experimental data points, and the dashed curve is the predicted trend. Reprinted with permission from Greiner *et al.*, Adv. Funct. Mater. **22**(21), 4557 (2012). Copyright 2012 Wiley.

function caused by an increase in the concentration of low electronegativity cations, and $\Delta\emptyset_d$ is the change in work function caused by an increase in the density of donor states. The term $\Delta\emptyset_x$ accounts for the gradual linear decline in the work function, and the term $\Delta\emptyset_d$ accounts for the initial rapid decrease in the work function with O-deficiency. The conductivity changes from insulating MoO_3 (10^{-7} S cm^{-1}) to metallic MoO_2 (10^4 S cm^{-1}) as the cation oxidation state decreases, which shows more than ten orders of enhancement. Figure 9 depicts the effects of the annealing temperature on the O/Mo ratio and the conductivity of the MoO_x film in N_2 and O_2.[56]

3. Contact resistivity and passivation of the HSL/n-Si interface

The carrier-selective properties of TMO/n-Si contacts are mainly evaluated via simultaneous consideration of the contact resistivity (ρ_c) and the recombination current parameter (J_{0c}). Note that current flows across the metal/TMO and TMO/n-Si interfaces, including the induced inversion layer on n-Si, such that ρ_c is the sum of the multiple contributions. Although still applicable to highly efficient c-Si solar cell designs, ρ_c and J_{0c} of MoO_x on n-Si (2.1 Ω cm) are quite high with optimum values of 30 mΩ cm^2 and 300 fA cm^2, respectively.[63] Gerling *et al.* extracted ρ_c values of 110 mΩ cm^2 (VO_x), 370 mΩ cm^2 (MoO_x), and 670 mΩ cm^2 (WO_x), all of which are close to the target series resistance values for most c-Si solar cells (0.1–0.5 Ω cm).[9]

Theoretically, the lattice mismatch between TMO and c-Si will inevitably result in a high defect density and consequently in a high carrier recombination at the contact interface. The HR-TEM images in Fig. 10 reveal the presence of an amorphous and relatively uniform silicon oxide layer at the TMO/c-Si interface, which provides a slight passivation effect.[64,65] Gerling *et al.* indicated that the formation of a SiO_2 layer is likely related to the chemical reaction with the TMOs during deposition and the maximum interlayer thickness is 2.8 nm (WO_3), 2.5 nm (MoO_3), and 2.2 nm (V_2O_5).[66] Further increasing the thickness of the SiO_x interlayer demonstrated a negligible influence on the surface passivation instead of introducing an increased contact resistivity.[67] As shown in Fig. 11, an efficiency over 16% has been obtained with the structure of MoO_x/SiO_x/n-Si.[68,69]

An additional ultrathin a-Si:H(i) interlayer between the c-Si surface and the TMO has frequently been investigated to further decrease the interfacial recombination.[5,14,34,48,70,71] An inferior effective carrier lifetime of below 500 μs was measured when the MoO_x

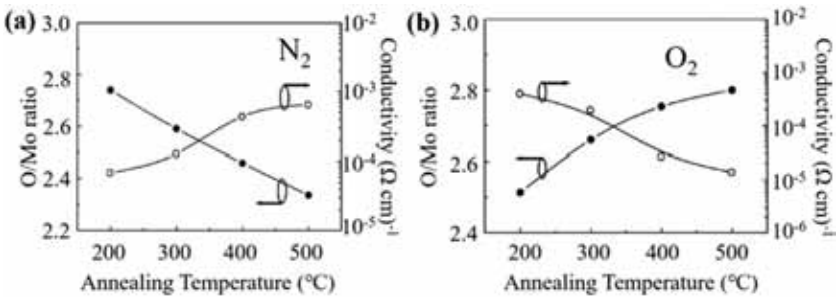

FIG. 9. Annealing temperature dependence of the O/Mo ratio and the conductivity of the MoO3 film in (a) N_2 and (b) O_2. Reprinted with permission from Lin *et al.*, Adv. Funct. Mater. **255**(6), 3868 (2009). Copyright 2009 Elsevier.

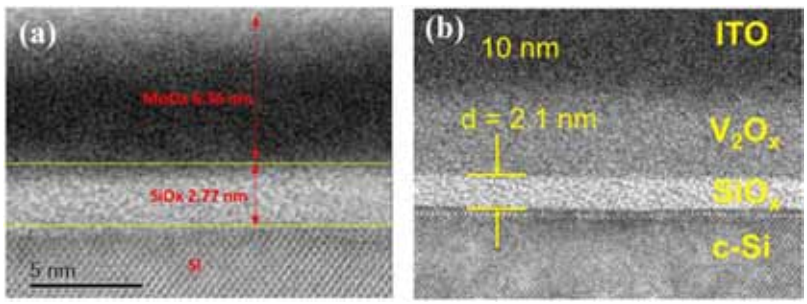

FIG. 10. HR-TEM images of the ITO/TMO/n-Si heterostructures showing an interlayer between n-Si and (a) MoO_x[65] and (b) V_2O_5.[64] (a) Reprinted with permission from Zhang *et al.*, J. Appl. Phys. **124**(7), 073106 (2018). Copyright 2018 AIP Publishing LLC. (b) Reprinted with permission from Gerlin *et al.*, Energy Procedia **124**, 584 (2017). Copyright 2017 Author(s), licensed under a Creative Commons Attribution 3.0 Unported License.

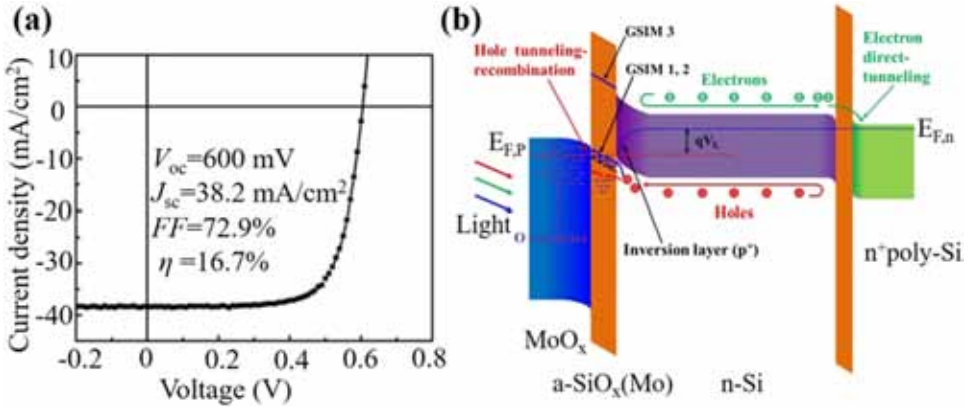

FIG. 11. (a) The J-V characteristic of the MoOx/n-Si device with surface texture, under the AM 1.5G illumination conditions. (b) The band diagram for the MoOx/a-SiOx(Mo)/n-Si device, at the open circuit state (nonequilibrium state) and under the illumination case. Reprinted with permission from Gao *et al.*, ACS Appl. Mater. Interfaces **10**(32), 27454 (2018). Copyright 2018 The American Chemical Society.

films were directly deposited on the Si surface by thermal evaporation. However, over 1 ms of lifetime and over 700 mV of V_{oc} would be obtained if an intrinsic a-Si:H passivation layer was adopted to form the MoOx/a-Si:H stack.[37,66,70]

C. High efficiency TMO/n-Si HSCs

1. Asymmetric heterocontacts

A power conversion efficiency of 22.5% has been achieved for the HSCs with an MoO_x hole-selective layer. An unsatisfied, doped-layer, i.e., a-Si:H(n), was still involved as a back surface field (BSF).[14] The dopant-free asymmetric heterocontact (DASH) solar cells based on TMOs usually adopt a both-side contacted front-junction structure. Bullock *et al.* first fabricated the DASH cell with an MoO_x/a-Si:H(i)/n-Si/a-Si:H(i)/LiF_x structure, showing an efficiency approaching 20%.[5] The latest reported conversion efficiency is 20.7%, with a structure of TCO/MoOx/a-Si:H(i)/n-Si/a-Si:H(i)/TiOx/LiF/Al, as shown in Fig. 12.[4] Imran's numerical simulation demonstrated that the theoretical efficiency for a both-side contacted DASH solar cell can be as high as 28%, with a V_{oc} of 772.7 mV, J_{sc} of 43.63 mA/cm^2, and *FF* of 82.99%.[42]

2. Interdigitated back contact (IBC)

Um *et al.* fabricated IBC solar cells by selectively depositing MoO_x and LiF_x films on the rear surfaces of the Si absorber and achieved a peak-to-correlation energy (PCE) of 15.4%.[72] With a very low temperature fabrication procedure, the Ni/V_2O_x stack was used to form the n-Si IBC HSC architecture. This Ni/V_2O_x-based IBC cell resulted in V_{oc}, J_{sc}, and *FF* values of 656 mV, 40.7 mA cm^2, and 74.0%, respectively, leading to a PCE as high as 19.7%.[67] Shen and co-workers investigated the electrical properties of typical TMO-based emitters in dopant-free n-Si IBC HSCs. Notably, the author only used two hard masks to complete the whole rear-sided processes and demonstrated a 22% efficiency by applying MoO_x and MgF_x as hole- and electron-selective contact layers,[73,74] respectively. This hard mask processing method shows huge potential for the simplification of the procedure over traditional doping techniques. As shown in Fig. 13, Shen *et al.* further presented a TMO/metal/TMO (TMT)[75,76] structure as a dopant-free hole-selective contact to reduce contact resistivity.[77,78] The efficiency of 19.2% and 15.8% was achieved by using V_2O_x (8 nm)/Au (4 nm)/V_2O_x (VMV) and CrO_x (5 nm)/Au (4 nm)/CrO_x as an emitter, respectively.

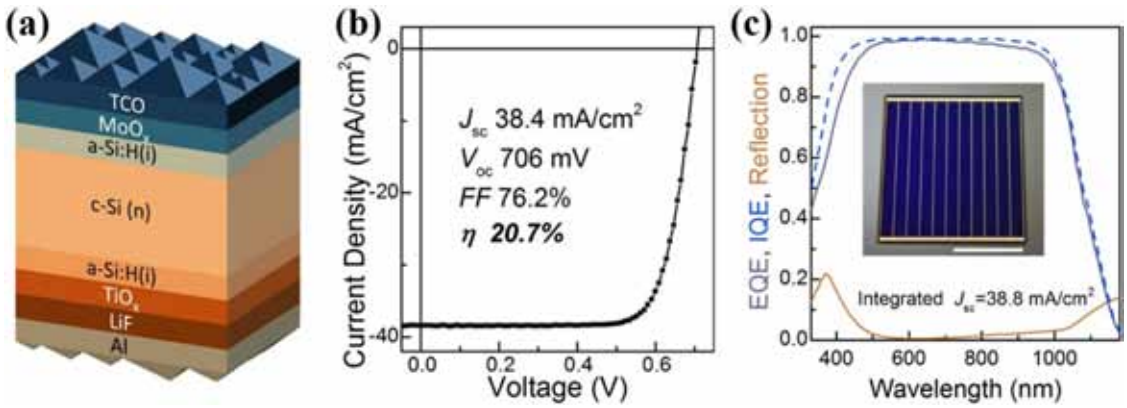

FIG. 12. DASH cell record. (a) Structure of the DASH cell, (b) 1-sun light *J-V* behavior of the champion DASH cell, and (c) external quantum efficiency (EQE), internal quantum efficiency (IQE), and reflection of the champion DASH cell; the inset shows a photograph of the cell design and the integrated J_{sc} value. The white scale bar is ~1 cm. Reprinted with permission from Bullock *et al.*, ACS Energy Lett. **3**(3), 508 (2018). Copyright 2018 American Chemical Society.

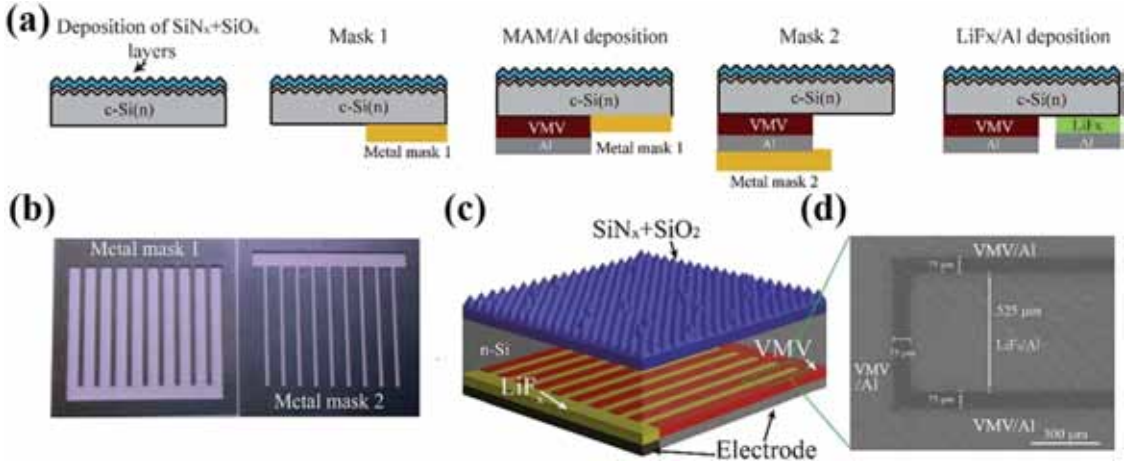

FIG. 13. (a) Schematic illustrating the MLBC solar cell metal patterning fabrication process. (b) The two metal patterning masks. (c) The structure of a completed MLBC solar cell. (d) SEM image of the results of metal mask patterning. Reprinted with permission from Wu *et al.*, RSC Adv. **7**(38), 23851 (2017). Copyright 2017 Royal Society of Chemistry.

D. Stability of TMO/Si HSCs

An efficiency of 22.5% has been achieved with a 7 nm MoO_x layer that was thermally evaporated on the a-Si:H(i) passivation layer. However, in that paper, 130 °C was found to be the upper limit on the processing temperature.[14] To circumvent the potential degradation from the following metallization process, a room temperature Cu electroplating metallization process was required to replace the traditional screen-printed Ag. Recent studies indicated that the performance of HSCs with TCO/MoO_x/a-Si:H(i) stacks degraded after annealing at temperatures from 130 °C to 200 °C, i.e., *FF* dropped from 76.6% to 69.7%[14] or PCE dropped from 12.6% to 11%[9] because of hydrogen diffusion. Neusel *et al.*[79] found that degradation in selectivity by MoO_x after annealing is caused by the reduction in the work function. This might be ascribed to the chemical or adsorption reactions of the samples with water and oxygen species. Masmitjà *et al.*[67] found that the V_2O_x/Si sample exhibited a better long-term surface passivation by coating a 10 nm Ni capping layer. However, subjecting as-fabricated solar cells with Ni and TCO capping layers to annealing at temperatures higher than 130 °C does cause negative effects on performance, which may be caused by interfacial reactions between V_2O_x and the Ni layer.

Zhang *et al.*[65,80,81] researched the materials of MoO_x during postdeposition annealing by *in situ* XPS/UPS investigations. They found that the MoO_x film degraded gradually with the increase in annealing temperature and the density of oxygen vacancies increased consequently. In addition, the degradation was found to be strongly dependent on the underlying layer.

IV. ALTERNATIVE MATERIALS FOR HETEROJUNCTION CONTACT

A. Graphene/Si

As a 2D material, graphene (Gr) has attracted significant attention in the development of high-performance photoelectronic devices due to its universal absorbance and extremely high carrier mobility.[82–85] Graphene films can be combined with Si to form Schottky junctions; hence, it can be used in Si-based solar cells. The Gr/Si solar cell was first reported by Wu *et al.* in 2010, as shown in Fig. 14. Figure 14(a) shows the energy diagram of the forward-biased graphene/n-Si Schottky junction upon illumination. Their Gr/Si solar cell achieved a photoelectric conversion efficiency of only 0.65%.[12]

Actually, the promotion of efficiency on Gr/Si solar cells faces the following three problems:

1. The relatively low Schottky barrier of the Gr/Si interface.
2. The high density of graphene defects formed during growth and transfer.
3. The severe recombination at the Gr/Si interface.

Great efforts were devoted to overcome these deficiencies, and so far, the device efficiency has been promoted from 1.65% to 16.2%.[86]

1. Optimization on light harvesting

For the conventional silicon solar cell, texturing and antireflection (AR) films are used to reduce optical loss. Surface texturing with nanostructures also have been used in the Gr/Si solar cell.[87–91] However, on the Gr/Si device, the graphene is transferred and liable to be destroyed by textured-Si. In addition, the efficiency of the Gr/Si solar cell was limited by the severe surface recombination due to a large specific surface area of Si nanostructures. Therefore, more successful light management engineering currently comes from antireflection coating, such as spin-coated TiO_2,[92] V_2O_5,[93] PMMA,[94] and fluoropolymer.[95] As shown in Fig. 15, Jie *et al.* introduced a MgF_2/ZnS multi-AR coating in the Gr/Si solar cell. An efficiency of 14.6% has been obtained by this means.[96]

2. Modification of graphene

At present, there are a large number of grain boundaries and defects in the graphene film deposited by the chemical vapor

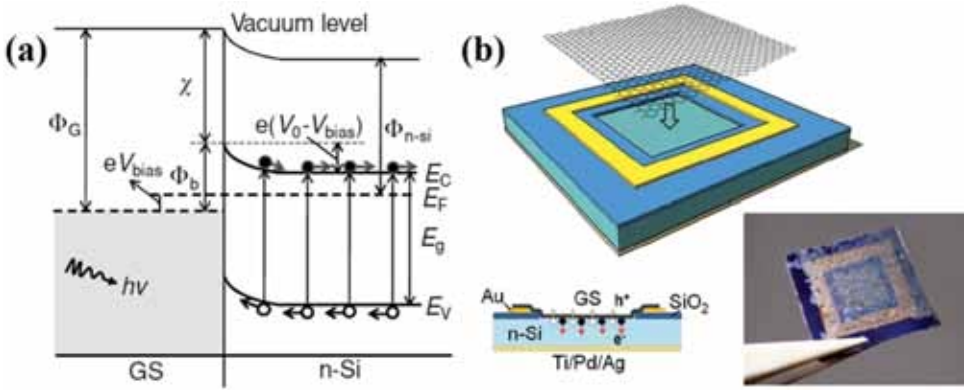

FIG. 14. (a) Energy diagram of a forward-biased GS/n-Si Schottky junction. (b) Schematic illustration of the device configuration. Reprinted with permission from Li *et al.*, Adv. Mater. **22**(25), 2743 (2010). Copyright 2010 Wiley.

deposition (CVD) method, and thus, the carrier mobility is far below the theoretical value. Moreover, they have a low carrier concentration and sheet conductivity, which greatly limits the performance of the Gr/Si solar cells. Moreover, the energy potential built by contacting intrinsic graphene with *n*-type silicon is insufficient, resulting in a large reverse saturation current J_0 and low *FF* and V_{oc}.

Gr is sensitive to molecular doping, e.g., it can be *p*-type doped with some strong oxidizing or electron attracting substances (TFSA,[97,98] $AuCl_3$,[91,99] and Au/Pt nanoparticles[100]) to increase the conductivity and work function. Another dopant such as graphene oxide (GO) not only provides *p*-type doping to Gr but also acts as an antireflection (AR) layer in the solar cell.[101] Ding *et al.* found that a several nanometer thick MoO_3 layer increased the work function of Gr in solar cells from 4.4 to 6.65 eV. As a result, V_{oc} of the device reached 0.57 V.[102]

3. Optimization of the Gr/Si interface

As a heterojunction device, interfacial recombination has always been one of the most important problems faced by researchers. Jie *et al.* performed hydrogen passivation, silicon oxide passivation (SiO_x), and methyl passivation (CH_3–Si) on Si to suppress carrier recombination at the Gr/Si interface.[103] Then, a layer of 3-hexylthiophene (P3HT) film was spin-coated on the silicon surface, which can block electrons and transport holes, thereby suppressing interfacial recombination and improving the built-in potential of the device. Yang *et al.* prepared a Gr/GO/Si solar cell with an insulating passivation layer of graphene oxide (GO).[104] When the thickness of GO is below 2.4 nm, carrier tunneling is not hindered, and V_{oc} gradually increases as increasing the GO thickness. Quantum dots are the other type optional material as the

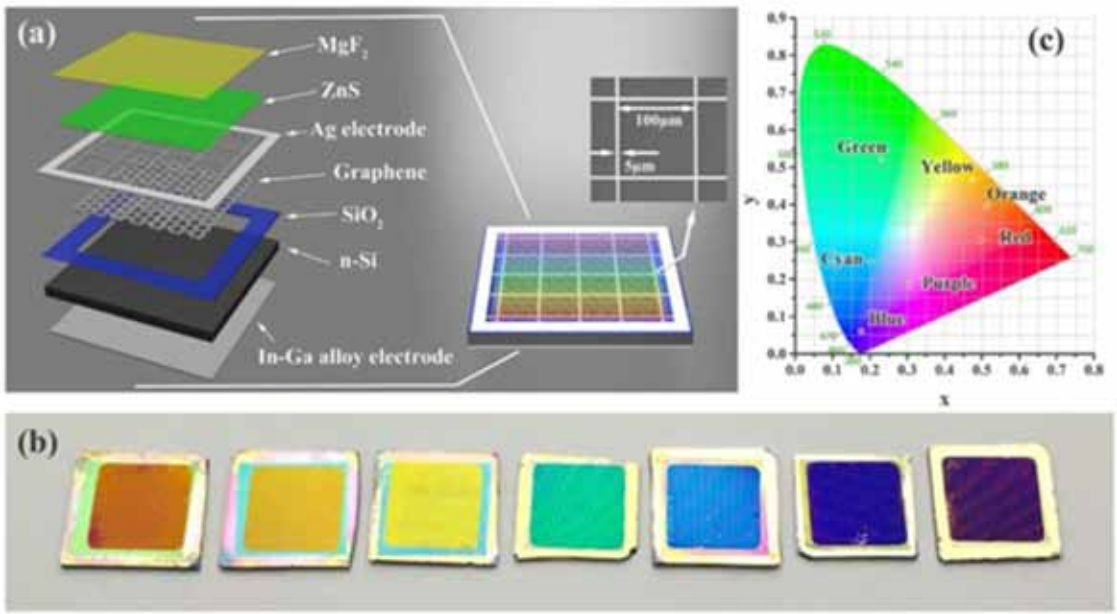

FIG. 15. (a) Schematic illustration of color Gr/Si heterojunction solar cells with MgF_2/ZnS films. (b) Photographs of Gr/Si heterojunction solar cells with different colors. (c) Coordinates of seven colors in CIE chromaticity. Reprinted with permission from Ding *et al.*, Nano Energy **46**, 257 (2018). Copyright 2018 Elsevier.

insertion layer. Kim *et al.* first inserted a layer of *p*-type doped Si quantum dots (*p*-SQDs) at the Gr/Si interface and received a great improvement in the efficiency. In this type of device, both *p*-SQDs and n-Si substrates absorb incident light, and two junctions effectively separate the photogenerated carriers. Finally, they demonstrated a record-breaking efficiency of 16.2%.[86]

B. PEDOT:PSS/Si

Conjugated polymer such as PEDOT:PSS is a promising organic candidate for organic/silicon heterojunction solar cells due to the excellent transparency, high conductivity (up to 1000 S/cm), suitable work function(4.8–5.2 eV), and nontoxic property.[105–108] When the PEDOT:PSS is in contact with n-Si, it will lead to an inversion layer at the side of silicon.[109–111] Therefore, this polymer exists as a *p*-type conductive material and a window electrode, which is similar to the scenario of TMOs.[112]

C. Light management

Suffering from severe optical reflection loss, planar c-Si only has 60% light absorption efficiency.[113] In the device of PEDOT:PSS/n-Si HSCs, the utilization of light can be enhanced by introduction of the textured-Si structure[114,115] and exterior antireflection layer,[116–119] lowering the overshadowing of the electrode grid[120–122] and reducing the parasitic absorption of the PEDOT:PSS.

Parasitic absorption can be suppressed largely by reducing the thickness of the PEDOT:PSS layer and moderately introducing additives such as sorbitol. Decreasing the overshadowing of the electrode grid[120] is an effective method to reduce optical loss. The morphology of textured-Si is varied, including black-silicon, pyramids, nanocones, and nanowire dual structures,[107,123–128] in order to achieve a low reflection. However, effective light trapping structures bring in disadvantages as well: (1) Enlarged surface area causes a great deal of defects, leading to deterioration of V_{oc}. (2) It is hard for PEDOT:PSS to form conformal coating at the textured-Si surface.[129]

Researchers devoted to conquer these dilemmas by the introduction of low aspect-ratio texturing structures,[130–136] surface modification,[137] and treatments with appropriate additives (into PEDOT:PSS solution).[134,138,139] As shown in Figs. 16(a) and 16(b), researchers developed a metal-assisted chemical etching method to recreate the texturing with hierarchically bowl-like nanopores[130,140,141] on n-Si, which realizes an omnidirectional light harvest over a broadband solar spectrum. In addition, transparent hole transporting organic small molecule SpiroOMeTAD,[142] TAPC,[143] TPD,[144] and inorganic layer (TiO_2)[145] was spin coated on Si nanowire (SiNW) arrays to infiltrate into the small gaps among the SiNWs and maximize the effective areas of heterojunction.[142] Moreover, the glycidoxypropyltrimethoxysilane (GOPS) additive was added into PEDOT:PSS to improve the contact properties between Si and PEDOT:PSS.[139,146] The device achieved obvious enhancement in optical harvest and junction quality. Finally, adding external force was found as an effective method to improve contact properties as well.[147] As shown in Fig. 16(c),[148] coating diethyl phthalate (DEP) onto PEDOT:PSS can stretch PEDOT:PSS to have a tight contact with n-Si, even at the bottom of the textured Si.

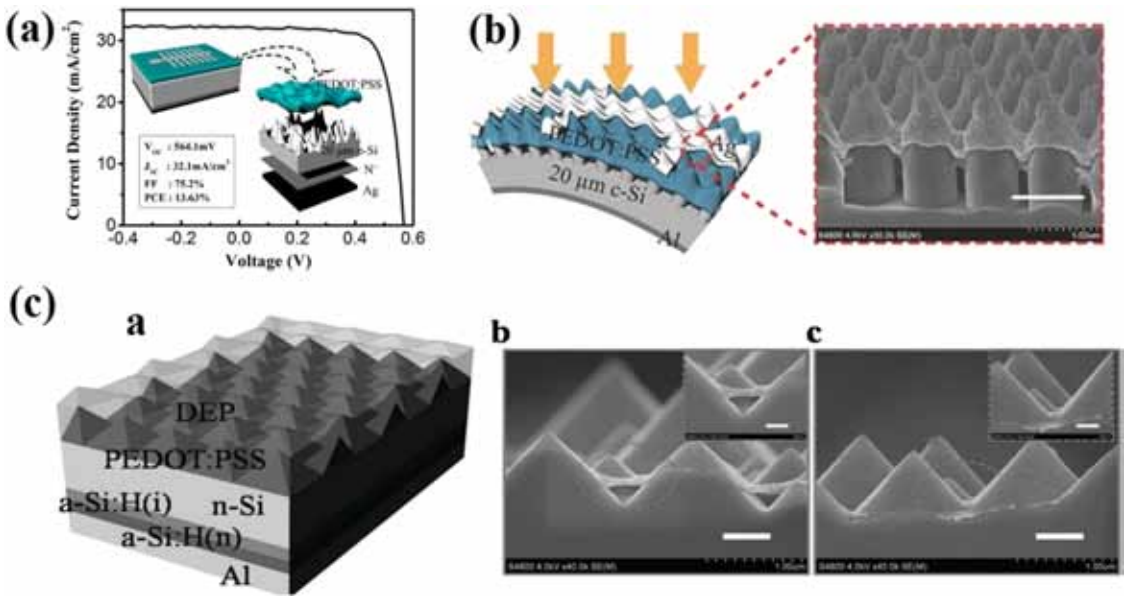

FIG. 16. (a) The device structures and the *J-V* curve of thin film c-Si/PEDOT:PSS hybrid solar cells with reconstructed-SiNPs. Reprinted with permission from He *et al.*, ACS Nano **9**, 6522 (2015). Copyright 2015 American Chemical Society. (b) Structure configuration of 20 μm PEDOT:PSS/n-Si HSCs with the NC-NP dual-structure as a light-trapping scheme. Reprinted with permission from He *et al.*, Adv. Energy Mater. **6**(8), 1501793 (2016). Copyright 2017 Wiley. (c) (a) Conceptual structure of the heterojunction solar cell with DEP coating. Cross-sectional scanning electron images of the as-fabricated n-Si/PEDOT:PSS junction on the textured-Si substrate without DEP coating (b) and with DEP coating (c). Reprinted with permission from He *et al.*, Adv. Mater. **29**(15), 1606321 (2017). Copyright 2017 Wiley.

Table I. Summary of the lasted efficiency of heterojunction solar cells with different hole selective contacts and architectures.

Heterojunction type	Device architecture	Area (cm^2)	PCE (%)
SHJ	TCO/a-Si:H(p/i)/n-Si/a-Si:H(i/n)/TCO[21]	152	25.1
	IBC-SHJ[3]	~180	26.6
TMO/Si	Cu/TCO/MoO_x/a-Si:H(i)/n-Si/a-Si:H(i/n)/Ag[14]	3.93	22.5
	Ag/TCO/MoO_x/a-Si:H(i)/n-Si/a-Si:H(i)/TiO_x/LiF/Al[4]	4	20.7
	Ag/TCO/MoO_x/a-SiO_x/n-Si/a-SiO_x/poly-Si/Al[69]	1	16.7
	MoO_x-based IBC[73]	4.5	22.2
	V_2O_x-based IBC[77]	4	19.2
	V_2O_x-based IBC[67]	16	19.7
Gr/Si	Al/Gr/p-SQDs/n-Si/Al[86]	1	16.2
PEDOT:PSS	Ag/bilayer-PEDOT:PSS/n-Si/CPTA/Al (front junction)[151]	1	16.7
	Ag/SiN_x/Al_2O_3/n^+-Si/n-Si/SiO_x/PEDOT:PSS/Ag (back junction)[169]	4	17.4
	PEDOT:PSS-based IBC[121]	1	16.3

D. Modification of PEDOT:PSS

The conductivity of the PEDOT:PSS shows anisotropy,[149] which is three orders of magnitude larger in the direction perpendicular to the substrate than that in the lateral direction. This is related to the spin-coating process, i.e., PEDOT enriching at the bottom side while PSS floating in the above because of water evaporation.[150] Typically, addition of dimethyl sulfoxide (DMSO) or ethylene glycol (EG) to the PEDOT:PSS solution yields improved conductivity (about 500 S/cm). He *et al.* provided a high-conductivity PEDOT:PSS (HC-PEDOT:PSS, 1500 S/cm) by doping PEDOT:PSS with an ionic liquid of 1-ethyl-3-methylimidazolium tricyanomethanide (EMIM/TCM).[151] The strategies of improving the work function of PEDOT:PSS were also used to improve the cell performance, for example, addition of foreign materials (such as perfluorinated ionomer[152]) into PEDOT:PSS or coating of high-WF materials (such as MoO_3[116] and CuI[153]) upon the PEDOT:PSS film.

E. Rear side contacts

Yang *et al.*[129] found that short circuit current is more sensitive to the rear interface than that of the front. The influence of the back side could be divided into passivation and contact resistivity. Generally, the n-Si/PEDOT:PSS HSCs are fabricated by directly depositing Al on the rear side to collect electrons. This will result in an inescapable Schottky barrier and severe charge recombination. In the dopant-free concept, an effective approach to realize Ohmic contact is by inserting an interfacial electron-selective layer (ESL). Metal oxides (e.g., MgO,[154] ZnO,[155] and SnO_2[156]), metal fluorides (e.g., LiF_x,[157,158] MgF_x[159]), organic materials (e.g., PFN,[160] N2200,[161,162] and PTB7[163]), and other low work function materials[164–167] have been reported as ESLs to remove the Fermi-level pinning effect and significantly enhance the electron extraction from the n-Si to the Al electrode. The passivating Si film by depositing hydrogenated amorphous silicon (a-Si:H) before electrode deposition can significantly increase the minority carrier lifetime due to a downward band bending for reflecting holes.[168]

V. SUMMARY

This article presents the latest advances in highly efficient Si-based heterojunction solar cells with various hole selective layers (HSLs). A record efficiency of 26.6% has been demonstrated by combining with the a-Si:H layer and IBC structure. A technological route combining carrier-selection, passivation contact, and IBC structure has been established to achieve even higher conversion efficiency. Beside the wide investigations on SHJ solar cells, the TMOs (i.e., MoO_x, V_2O_x, and WO_x), PEDOT:PSS, and graphene with high work functions have critical applications in heterojunction solar cells as promising candidates for replacement of the a-Si:H(p) layer. These dopant-free HSCs show a great potential for high efficiency and low-cost. In order to optimize the performance of HSL/Si solar cells, great efforts have been comprehensively summarized, including the exploitation of advanced designs for devices, modification of hole-selective materials (work function and conductivity), and interfacial passivation. Moreover, TMOs have been integrated into IBC HSCs, realizing the aim of gentle fabrication methods and high efficiency. The lasted efficiencies of heterojunction solar cells were summarized and shown in Table I. Despite the rapid progress of dopant-free HSCs recently, there are still several important issues needed to be solved, e.g., the stability of device and the compatibility of TMOs with screen-printed technology.

ACKNOWLEDGMENTS

P.G. acknowledges the support of National Natural Science Foundation of China (Grant Nos. 61974169 and 61674154) and Zhejiang Provincial Natural Science Foundation (Grant No. LR19E020001). S.P. acknowledges the support of Key Areas Scientific and Technological Research Projects in Xinjiang Production and Construction Corps (Grant No. 2018AB004). M.L. acknowledges the support of the Par-Eu Scholars Program, Science and Technology Beijing 100 Leading Talent Training Project.

REFERENCES

[1]X. Yang, H. Ali, Q. Bi, K. Davis, W. V. Schoenfeld, and K. Weber, Adv. Mater. **28**(28), 5891 (2016).
[2]M. A. Green, Y. Hishikawa, E. D. Dunlop, D. H. Levi, J. Hohl-Ebinger, M. Yoshita, and A. W. Y. Ho-Baillie, Prog. Photovoltaics: Res. Appl. **27**(1), 3 (2019).
[3]K. Yoshikawa, W. Yoshida, T. Irie, H. Kawasaki, K. Konishi, H. Ishibashi, T. Asatani, D. Adachi, M. Kanematsu, H. Uzu, and K. Yamamoto, Sol. Energy Mater. Sol. Cells **173**, 37 (2017).
[4]J. Bullock, Y. Wan, Z. Xu, S. Essig, M. Hettick, H. Wang, W. Ji, M. Boccard, A. Cuevas, C. Ballif, and A. Javey, ACS Energy Lett. **3**(3), 508 (2018).
[5]J. Bullock, M. Hettick, J. Geissbühler, A. J. Ong, T. Allen, C. M. Sutter-Fella, T. Chen, H. Ota, E. W. Schaler, S. De Wolf, C. Ballif, A. Cuevas, and A. Javey, Nat. Energy **1**(3), 15031 (2016).
[6]K. Mallem, Y. J. Kim, S. Q. Hussain, S. Dutta, A. H. T. Le, M. Ju, J. Park, Y. H. Cho, Y. Kim, E.-C. Cho, and J. Yi, Mater. Res. Bull. **110**, 90 (2019).
[7]M. Bivour, J. Temmler, H. Steinkemper, and M. Hermle, Sol. Energy Mater. Sol. Cells **142**, 34 (2015).
[8]S. Q. Hussain, K. Mallem, M. A. Khan, M. Q. Khokhar, Y. Lee, J. Park, K. S. Lee, Y. Kim, E. C. Cho, Y. H. Cho, and J. Yi, Trans. Electr. Electron. Mater. **20**(1), 1 (2018).
[9]L. Gerling, S. Mahato, C. Voz, R. Alcubilla, and J. Puigdollers, Appl. Sci. **5**(4), 695 (2015).
[10]Q. Liu, I. Khatri, R. Ishikawa, K. Ueno, and H. Shirai, Phys. Status Solidi C **9**(10-11), 2101 (2012).
[11]J. P. Thomas and K. T. Leung, Adv. Funct. Mater. **24**(31), 4978 (2014).
[12]X. Li, H. Zhu, K. Wang, A. Cao, J. Wei, C. Li, Y. Jia, Z. Li, X. Li, and D. Wu, Adv. Mater. **22**(25), 2743 (2010).
[13]K. Huang, X. Yu, J. Cong, and D. Yang, Adv. Mater. Interfaces **5**(24), 1801520 (2018).
[14]J. Geissbühler, J. Werner, S. Martin de Nicolas, L. Barraud, A. Hessler-Wyser, M. Despeisse, S. Nicolay, A. Tomasi, B. Niesen, S. De Wolf, and C. Ballif, Appl. Phys. Lett. **107**(8), 081601 (2015).
[15]M. Taguchi, M. Tanaka, T. Matsuyama, T. Matsuoka, S. Tsuda, S. Nakano, Y. Kishi, and Y. Kuwano, in *Digest 5th International Photovoltaic Science and Engineering Conference* (Elsevier, Kyoto, Japan, 1990), p. 689.
[16]M. Tanaka, M. Taguchi, T. Matsuyama, T. Sawada, S. Tsuda, S. Nakano, H. Hanafusa, and Y. Kuwano, Jpn. J. Appl. Phys. **31**, 3518 (1992).
[17]J. I. Pankove and M. L. Tarng, Appl. Phys. Lett. **34**(2), 156 (1979).
[18]S. Olibet, E. Vallat-Sauvain, and C. Ballif, Phys. Rev. B **76**(3), 035326 (2007).
[19]C. Battaglia, A. Cuevas, and S. D. Wolf, Energy Environ. Sci. **9**, 1552 (2016).
[20]M. Taguchi, A. Yano, S. Tohoda, K. Matsuyama, Y. Nakamura, T. Nishiwaki, K. Fujita, and E. Maruyama, IEEE J. Photovoltaics **4**(1), 96 (2014).
[21]D. Adachi, J. L. Hernández, and K. Yamamoto, Appl. Phys. Lett. **107**(23), 233506 (2015).
[22]D. D. Smith, P. Cousins, S. Westerberg, R. D. Jesus-Tabajonda, G. Aniero, and Y.-C. Shen, IEEE J. Photovoltaics **4**(6), 1465 (2014).
[23]M. D. Lammert and R. J. Schwartz, IEEE Trans. Electron Devices **24**, 337 (1977).
[24]M. Lu, S. Bowden, U. Das, and R. Birkmire, Appl. Phys. Lett. **91**(6), 063507 (2007).
[25]S.-Y. Lee, H. Choi, H. Li, K. Ji, S. Nam, J. Choi, S.-W. Ahn, H.-M. Lee, and B. Park, Sol. Energy Mater. Sol. Cells **120**, 412 (2014).
[26]N. Mingirulli, J. Haschke, R. Gogolin, R. Ferré, T. F. Schulze, J. Düsterhöft, N.-P. Harder, L. Korte, R. Brendel, and B. Rech, Phys. Status Solidi RRL **5**(4), 159 (2011).
[27]K. Masuko, M. Shigematsu, T. Hashiguchi, D. Fujishima, M. Kai, N. Yoshimura, T. Yamaguchi, Y. Ichihashi, T. Mishima, N. Matsubara, T. Yamanishi, T. Takahama, M. Taguchi, E. Maruyama, and S. Okamoto, IEEE J. Photovoltaics **4**(6), 1433 (2014).
[28]A. Tomasi, B. Paviet-Salomon, Q. Jeangros, J. Haschke, G. Christmann, L. Barraud, A. Descoeudres, J. P. Seif, S. Nicolay, M. Despeisse, S. D. Wolf, and C. Ballif, Nat. Energy **2**, 17062 (2017).
[29]K. Yoshikawa, H. Kawasaki, W. Yoshida, T. Irie, K. Konishi, K. Nakano, T. Uto, D. Adachi, M. Kanematsu, H. Uzu, and K. Yamamoto, Nat. Energy **2**(5), 17032 (2017).
[30]R. V. K. Chavali, S. De Wolf, and M. A. Alam, Prog. Photovoltaics: Res. Appl. **26**(4), 241 (2018).
[31]Z. C. Holman, A. Descoeudres, L. Barraud, F. Z. Fernandez, J. P. Seif, S. De Wolf, and C. Ballif, IEEE J. Photovoltaics **2**(1), 7 (2012).
[32]A. Richter, F. Werner, A. Cuevas, J. Schmidt, and S. W. Glunz, Energy Procedia **27**, 88 (2012).
[33]Y. Wan, S. K. Karuturi, C. Samundsett, J. Bullock, M. Hettick, D. Yan, J. Peng, P. R. Narangari, S. Mokkapati, H. H. Tan, C. Jagadish, A. Javey, and A. Cuevas, ACS Energy Lett. **3**, 125 (2018).
[34]F. Wang, S. Zhao, B. Liu, Y. Li, Q. Ren, R. Du, N. Wang, C. Wei, X. Chen, G. Wang, B. Yan, Y. Zhao, and X. Zhang, Nano Energy **39**, 437 (2017).
[35]R. Peibst, Y. Larionova, S. Reiter, T. F. Wietler, N. Orlowski, S. Schafer, B. Min, M. Stratmann, D. Tetzlaff, J. Krugener, U. Hohne, J. D. Kahler, H. Mehlich, S. Frigge, and R. Brendel, IEEE J. Photovoltaics **8**(3), 719 (2018).
[36]L. G. Gerling, S. Mahato, A. Morales-Vilches, G. Masmitja, P. Ortega, C. Voz, R. Alcubilla, and J. Puigdollers, Sol. Energy Mater. Sol. Cells **145**, 109 (2016).
[37]L. G. Gerling, G. Masmitja, C. Voz, P. Ortega, J. Puigdollers, and R. Alcubilla, Energy Procedia **92**, 633 (2016).
[38]O. Almora, L. G. Gerling, C. Voz, R. Alcubilla, J. Puigdollers, and G. Garcia-Belmonte, Sol. Energy Mater. Sol. Cells **168**, 221 (2017).
[39]J. Tong, Y. Wan, J. Cui, S. Lim, N. Song, and A. Lennon, Appl. Surf. Sci. **423**, 139 (2017).
[40]C. Battaglia, X. Yin, M. Zheng, I. D. Sharp, T. Chen, S. McDonnell, A. Azcatl, C. Carraro, B. Ma, R. Maboudian, R. M. Wallace, and A. Javey, Nano Lett. **14**(2), 967 (2014).
[41]F. Wang, Z. Tan, and Y. Li, Energy Environ. Sci. **8**(4), 1059 (2015).
[42]H. Imran, T. M. Abdolkader, and N. Z. Butt, IEEE Trans. Electron Devices **63**(9), 3584 (2016).
[43]S. Q. Hussain, K. Mallem, Y. J. Kim, A. H. Tuan Le, M. Q. Khokhar, S. Kim, S. Dutta, S. Sanyal, Y. Kim, J. Park, Y. Lee, Y. H. Cho, E. C. Cho, and J. Yi, Mater. Sci. Semicond. Process. **91**, 267 (2019).
[44]R. García-Hernansanz, E. García-Hemme, D. Montero, J. Olea, A. del Prado, I. Mártil, C. Voz, L. G. Gerling, J. Puigdollers, and R. Alcubilla, Sol. Energy Mater. Sol. Cells **185**, 61 (2018).
[45]S. Essig, J. Dreon, E. Rucavado, M. Mews, T. Koida, M. Boccard, J. Werner, J. Geissbuhler, P. Loper, M. Morales-Masis, L. Korte, S. De Wolf, and C. Ballif, Sol. RRL **2**(4), 1700227 (2018).
[46]C. Lu, Rusli, A. B. Prakoso, and Z. Li, in *IEEE 7th World Conference on Photovoltaic Energy Conversion (WCPEC)* (IEEE, HI, USA, 2018), p. 2155.
[47]P. Gao, Z. Yang, J. He, J. Yu, P. Liu, J. Zhu, Z. Ge, and J. Ye, Adv. Sci. **5**(3), 1700547 (2018).
[48]C. Battaglia, S. M. de Nicolás, S. De Wolf, X. Yin, M. Zheng, C. Ballif, and A. Javey, Appl. Phys. Lett. **104**(11), 113902 (2014).
[49]T. Sun, R. Wang, R. Liu, C. Wu, Y. Zhong, Y. Liu, Y. Wang, Y. Han, Z. Xia, Y. Zou, T. Song, N. Koch, S. Duhm, and B. Sun, Phys. Status Solidi RRL **11**(7), 1700107 (2017).
[50]R. A. Vijayan, S. Essig, S. De Wolf, B. G. Ramanathan, P. Loper, C. Ballif, and M. Varadharajaperumal, IEEE J. Photovoltaics **8**(2), 473 (2018).
[51]C. Messmer, M. Bivour, J. Schön, and M. Hermle, J. Appl. Phys. **124**(8), 085702 (2018).
[52]C. Messmer, M. Bivour, J. Schon, S. W. Glunz, and M. Hermle, IEEE J. Photovoltaics **8**(2), 456 (2018).
[53]M. Mews, L. Korte, and B. Rech, Sol. Energy Mater. Sol. Cells **158**, 77 (2016).
[54]M. T. Greiner, M. G. Helander, W. M. Tang, Z. B. Wang, J. Qiu, and Z. H. Lu, Nat. Mater. **11**(1), 76 (2011).
[55]M. T. Greiner, L. Chai, M. G. Helander, W.-M. Tang, and Z.-H. Lu, Adv. Funct. Mater. **22**(21), 4557 (2012).
[56]S.-Y. Lin, Y.-C. Chen, C.-M. Wang, P.-T. Hsieh, and S.-C. Shih, Appl. Surf. Sci. **255**(6), 3868 (2009).
[57]F. Menchini, L. Serenelli, L. Martini, M. Izzi, G. Stracci, P. Mangiapane, E. Salza, and M. Tucci, Appl. Phys. A **124**(7), 489 (2018).

[58]B. Macco, M. F. J. Vos, N. F. W. Thissen, A. A. Bol, and W. M. M. Kessels, Phys. Status Solidi RRL **9**(7), 393 (2015).
[59]J. Ziegler, M. Mews, K. Kaufmann, T. Schneider, A. N. Sprafke, L. Korte, and R. B. Wehrspohn, Appl. Phys. A **120**, 811 (2015).
[60]R. G. Gordon, S. Barry, J. T. Barton, and R. N. R. Broomhall-Dillard, Thin Solid Films **392**, 231 (2001).
[61]R. U. Kirss and L. Meda, Appl. Organomet. Chem. **12**, 155 (1998).
[62]H. Simchi, B. E. McCandless, T. Meng, J. H. Boyle, and W. N. Shafarman, J. Appl. Phys. **114**(1), 013503 (2013).
[63]J. Bullock, A. Cuevas, T. Allen, and C. Battaglia, Appl. Phys. Lett. **105**(23), 232109 (2014).
[64]L. G. Gerlin, G. Masmitja, P. Ortega, C. Voz, R. Alcubilla, and J. Puigdollers, Energy Procedia **124**, 584 (2017).
[65]T. Zhang, C.-Y. Lee, Y. Wan, S. Lim, and B. Hoex, J. Appl. Phys. **124**(7), 073106 (2018).
[66]L. G. Gerling, C. Voz, R. Alcubilla, and J. Puigdollers, J. Mater. Res. **32**(2), 260 (2016).
[67]G. Masmitjà, L. G. Gerling, P. Ortega, J. Puigdollers, I. Martín, C. Voz, and R. Alcubilla, J. Mater. Chem. A **5**(19), 9182 (2017).
[68]J. Bullock, D. Yan, A. Cuevas, Y. Wan, and C. Samundsett, Energy Procedia **77**, 446 (2015).
[69]M. Gao, D. Chen, B. Han, W. Song, M. Zhou, X. Song, F. Xu, L. Zhao, Y. Li, and Z. Ma, ACS Appl. Mater. Interfaces **10**(32), 27454 (2018).
[70]D. Sacchetto, Q. Jeangros, G. Christmann, L. Barraud, A. Descoeudres, J. Geissbuhler, M. Despeisse, A. Hessler-Wyser, S. Nicolay, and C. Ballif, IEEE J. Photovoltaics **7**(6), 1584 (2017).
[71]M. A. Sen, P. Spinelli, B. Kikkert, E. Hoek, B. Macco, A. Weeber, and P. Bronsveld, in The 8th International Conference on Crystalline Silicon Photovoltaics, SiliconPV 2018, 2018.
[72]H. D. Um, N. Kim, K. Lee, I. Hwang, J. H. Seo, and K. Seo, Nano Lett. **16**(2), 981 (2016).
[73]W. Wu, W. Lin, S. Zhong, B. Paviet-Salomon, M. Despeisse, Z. Liang, M. Boccard, H. Shen, and C. Ballif, in the 8th International Conference on Crystalline Silicon Photovoltaics, SiliconPV 2018, 2018.
[74]W. Wu, J. Bao, X. Jia, Z. Liu, L. Cai, B. Liu, J. Song, and H. Shen, Phys. Status Solidi RRL **10**(9), 662 (2016).
[75]W. Wu, J. Bao, Z. Liu, W. Lin, X. Yu, L. Cai, B. Liu, J. Song, and H. Shen, Mater. Lett. **189**, 86 (2017).
[76]W. Lin, W. Wu, Z. Liu, K. Qiu, L. Cai, Z. Yao, B. Ai, Z. Liang, and H. Shen, ACS Appl. Mater. Interfaces **10**(16), 13645 (2018).
[77]W. Wu, W. Lin, J. Bao, Z. Liu, B. Liu, K. Qiu, Y. Chen, and H. Shen, RSC Adv. **7**(38), 23851 (2017).
[78]W. Lin, W. Wu, J. Bao, Z. Liu, K. Qiu, L. Cai, Z. Yao, Y. Deng, Z. Liang, and H. Shen, Mater. Res. Bull. **103**, 77 (2018).
[79]L. Neusel, M. Bivour, and M. Hermle, Energy Procedia **124**, 425 (2017).
[80]T. Zhang, C.-Y. Lee, B. Gong, and B. Hoex, in *the 8th International Conference on Crystalline Silicon Photovoltaics* (AIP Publishing, 2018), Vol. 1999, p. 040027.
[81]T. Zhang, C.-Y. Lee, B. Gong, S. Lim, S. Wenham, and B. Hoex, J. Vac. Sci. Technol., A **36**(3), 031601 (2018).
[82]Y. W. Tan, Y. Zhang, H. L. Stormer, and P. Kim, Eur. Phys. J.: Spec. Top. **148**(1), 15 (2007).
[83]A. A. Balandin, Nat. Mater. **10**(8), 569 (2011).
[84]A. K. Geim and K. S. Novoselov, Nat. Mater. **6**, 183 (2007).
[85]E. H. Hwang, S. Adam, and S. D. Sarma, Phys. Rev. Lett. **98**(18), 186806 (2007).
[86]J. M. Kim, S. Kim, D. H. Shin, S. W. Seo, H. S. Lee, J. H. Kim, C. W. Jang, S. S. Kang, S.-H. Choi, G. Y. Kwak, K. J. Kim, H. Lee, and H. Lee, Nano Energy **43**, 124 (2018).
[87]M. D. Kelzenberg, S. W. Boettcher, J. A. Petykiewicz, D. B. Turner-Evans, M. C. Putnam, E. L. Warren, J. M. Spurgeon, R. M. Briggs, N. S. Lewis, and H. A. Atwater, Nat. Mater. **9**(4), 368 (2010).
[88]T. Feng, D. Xie, Y. Lin, Y. Zang, T. Ren, R. Song, H. Zhao, H. Tian, X. Li, H. Zhu, and L. Liu, Appl. Phys. Lett. **99**(23), 233505 (2011).
[89]T. Feng, D. Xie, Y. Lin, H. Zhao, Y. Chen, H. Tian, T. Ren, X. Li, Z. Li, K. Wang, D. Wu, and H. Zhu, Nanoscale **4**(6), 2130 (2012).
[90]C. Xie, P. Lv, B. Nie, J. Jie, X. Zhang, Z. Wang, P. Jiang, Z. Hu, L. Luo, Z. Zhu, L. Wang, and C. Wu, Appl. Phys. Lett. **99**(13), 133113 (2011).
[91]C. Xie, X. Zhang, K. Ruan, Z. Shao, S. S. Dhaliwal, L. Wang, Q. Zhang, X. Zhang, and J. Jie, J. Mater. Chem. A **1**(48), 15348 (2013).
[92]E. Shi, H. Li, L. Yang, L. Zhang, Z. Li, P. Li, Y. Shang, S. Wu, X. Li, J. Wei, K. Wang, H. Zhu, D. Wu, Y. Fang, and A. Cao, Nano Lett. **13**(4), 1776 (2013).
[93]M. F. Bhopal, D. w. Lee, M. A. Rehman, Y. Seo, and S. H. Lee, Mater. Sci. Semicond. Process. **86**, 146 (2018).
[94]T. Jiao, D. Wei, X. Song, T. Sun, J. Yang, L. Yu, Y. Feng, W. Sun, W. Wei, H. Shi, C. Hu, and C. Du, RSC Adv. **6**(12), 10175 (2016).
[95]X. Gan, R. Lv, H. Zhu, L.-P. Ma, X. Wang, Z. Zhang, Z.-H. Huang, H. Zhu, W. Ren, M. Terrones, and F. Kang, J. Mater. Chem. A **4**(36), 13795 (2016).
[96]K. Ding, X. Zhang, L. Ning, Z. Shao, P. Xiao, A. Ho-Baillie, X. Zhang, and J. Jie, Nano Energy **46**, 257 (2018).
[97]F. Schedin, A. K. Geim, S. V. Morozov, E. W. Hill, P. Blake, M. I. Katsnelson, and K. S. Novoselov, Nat. Mater. **6**(9), 652 (2007).
[98]X. Miao, S. Tongay, M. K. Petterson, K. Berke, A. G. Rinzler, B. R. Appleton, and A. F. Hebard, Nano Lett. **12**(6), 2745 (2012).
[99]X. Li, D. Xie, H. Park, M. Zhu, T. H. Zeng, K. Wang, J. Wei, D. Wu, J. Kong, and H. Zhu, Nanoscale **5**(5), 1945 (2013).
[100]X. Liu, X. W. Zhang, J. H. Meng, Z. G. Yin, L. Q. Zhang, H. L. Wang, and J. L. Wu, Appl. Phys. Lett. **106**(23), 233901 (2015).
[101]S. Yavuz, C. Kuru, D. Choi, A. Kargar, S. Jin, and P. R. Bandaru, Nanoscale **8**(12), 6473 (2016).
[102]K. Ding, X. Zhang, F. Xia, R. Wang, Y. Kuang, S. Duhm, J. Jie, and X. Zhang, J. Mater. Chem. A **5**(1), 285 (2017).
[103]C. Xie, X. Zhang, Y. Wu, X. Zhang, X. Zhang, Y. Wang, W. Zhang, P. Gao, Y. Han, and J. Jie, J. Mater. Chem. A **1**(30), 8567 (2013).
[104]L. Yang, X. Yu, M. Xu, H. Chen, and D. Yang, J. Mater. Chem. A **2**(40), 16877 (2014).
[105]B. R. Lee, J.-W. Kim, D. Kang, D. W. Lee, S.-J. Ko, H. J. Lee, C.-L. Lee, J. Y. Kim, H. S. Shin, and M. H. Song, ACS Nano **6**, 2984 (2012).
[106]D. Alemu, H. Y. Wei, K. C. Ho, and C. W. Chu, Energy Environ. Sci. **5**(11), 9662 (2012).
[107]W. R. Wei, M. L. Tsai, S. T. Ho, S. H. Tai, C. R. Ho, S. H. Tsai, C. W. Liu, R. J. Chung, and J. H. He, Nano Lett. **13**(8), 3658 (2013).
[108]L. He, D. Lai, H. Wang, C. Jiang, and Rusli, Small **8**(11), 1664 (2012).
[109]W. J. Royea, A. Juang, and N. S. Lewis, Appl. Phys. Lett. **77**, 13 (2000).
[110]S. Jackle, M. Mattiza, M. Liebhaber, G. Bronstrup, M. Rommel, K. Lips, and S. Christiansen, Sci. Rep. **5**, 13008 (2015).
[111]A. S. Erickson, A. Zohar, and D. Cahen, Adv. Energy Mater. **4**(9), 1301724 (2014).
[112]M. Pietsch, S. Jäckle, and S. Christiansen, Appl. Phys. A **115**(4), 1109 (2014).
[113]F. Teng, N. Li, L. Liu, D. Xu, D. Xiao, and N. Lu, RSC Adv. **6**, 15803 (2016).
[114]Y. Li, M. Li, R. Li, P. Fu, T. Wang, Y. Luo, J. M. Mbengue, and M. Trevor, Sci. Rep. **6**, 24847 (2016).
[115]F. Bai, M. C. Li, R. Huang, Y. F. Li, M. Trevor, and K. P. Musselman, RSC Adv. **4**(4), 1794 (2014).
[116]R. Liu, S. T. Lee, and B. Sun, Adv. Mater. **26**(34), 6007 (2014).
[117]Q. Liu, R. Ishikawa, S. Funada, T. Ohki, K. Ueno, and H. Shirai, Adv. Energy Mater. **5**(17), 1500744 (2015).
[118]Y. Sun, Z. Yang, P. Gao, J. He, X. Yang, J. Sheng, S. Wu, Y. Xiang, and J. Ye, Nanoscale Res. Lett. **11**(1), 356 (2016).
[119]Z. Liu, Z. Yang, S. Wu, J. Zhu, W. Guo, J. Sheng, J. Ye, and Y. Cui, ACS Nano **11**(12), 12687 (2017).
[120]H.-D. Um, I. Hwang, N. Kim, Y. J. Yu, M. Wober, K.-H. Kim, and K. Seo, Adv. Mater. Interfaces **2**, 1500347 (2015).
[121]H. Lin, D. Ding, Z. Wang, L. Zhang, F. Wu, J. Yu, P. Gao, J. Ye, and W. Shen, Nano Energy **50**, 777 (2018).
[122]Z. Yang, H. Lin, K. W. A. Chee, P. Gao, and J. Ye, Nano Energy **61**, 221 (2019).
[123]Y. Da, X. Liu, Y. Xuan, and Q. Li, Int. J. Energy Res. **42**(15), 4875 (2018).
[124]S. Jeong, E. C. Garnett, S. Wang, Z. Yu, S. Fan, M. L. Brongersma, M. D. McGehee, and Y. Cui, Nano Lett. **12**(6), 2971 (2012).

[125]H. Wang, J. Wang, and Rusli, Nanoscale Res. Lett. **10**, 191 (2015).
[126]Z. Q. Ying, M. D. Liao, X. Yang, C. Han, J. Q. Li, J. S. Li, Y. L. Li, P. Q. Gao, and J. C. Ye, IEEE J. Photovoltaics **6**(4), 888 (2016).
[127]P. Gao, H. Wang, Z. Sun, W. Han, J. Li, and J. Ye, Appl. Phys. Lett. **103**(25), 253105 (2013).
[128]F. Bai, M. Li, R. Huang, D. Song, B. Jiang, and Y. Li, Nanoscale Res. Lett. **7**, 557 (2012).
[129]Z. Yang, P. Gao, J. He, W. Chen, W.-Y. Yin, Y. Zeng, W. Guo, J. Ye, and Y. Cui, ACS Energy Lett. **2**(3), 556 (2017).
[130]X. Yu, X. Shen, X. Mu, J. Zhang, B. Sun, L. Zeng, L. Yang, Y. Wu, H. He, and D. Yang, Sci. Rep. **5**, 17371 (2015).
[131]X. Wang, Z. Yang, P. Gao, X. Yang, S. Zhou, D. Wang, M. Liao, P. Liu, Z. Liu, S. Wu, J. Ye, and T. Yu, Opt. Express **25**(9), 10464 (2017).
[132]P. Gao, J. He, S. Zhou, X. Yang, S. Li, J. Sheng, D. Wang, T. Yu, J. Ye, and Y. Cui, Nano Lett. **15**(7), 4591 (2015).
[133]Z. Wang, S. Peng, Y. Wen, T. Qin, Q. Liu, D. He, and G. Cao, Nano Energy **41**, 519 (2017).
[134]S.-S. Yoon and D.-Y. Khang, Adv. Energy Mater. **8**(9), 1702655 (2018).
[135]J. Zhang, T. Song, X. Shen, X. Yu, S.-T. Lee, and B. Sun, ACS Nano **8**, 11369 (2014).
[136]F. Bai, Y. Zhang, Z. Duan, R. Hoye, M. Trevor, Y. Li, and M. Li, AIP Adv. **7**(9), 095006 (2017).
[137]X. Dai, T. Chen, H. Cai, H. Wen, and Y. Sun, ACS Appl. Mater. Interfaces **8**(23), 14572 (2016).
[138]X. Shen, B. Sun, D. Liu, and S. T. Lee, J. Am. Chem. Soc. **133**(48), 19408 (2011).
[139]S. Wu, W. Cui, N. Aghdassi, T. Song, S. Duhm, S.-T. Lee, and B. Sun, Adv. Funct. Mater. **26**(28), 5035 (2016).
[140]J. He, P. Gao, M. Liao, X. Yang, Z. Ying, S. Zhou, J. Ye, and Y. Cui, ACS Nano **9**, 6522 (2015).
[141]J. He, Z. Yang, P. Liu, S. Wu, P. Gao, M. Wang, S. Zhou, X. Li, H. Cao, and J. Ye, Adv. Energy Mater. **6**(8), 1501793 (2016).
[142]L. He, C. Jiang, Rusli, D. Lai, and H. Wang, Appl. Phys. Lett. **99**(2), 021104 (2011).
[143]P. Yu, C.-Y. Tsai, J.-K. Chang, C.-C. Lai, P.-H. Chen, Y.-C. Lai, P.-T. Tsai, M.-C. Li, H.-T. Pan, Y.-Y. Huang, C.-I. Wu, Y.-L. Chueh, S.-W. Chen, C.-H. Du, S.-F. Horng, and H.-F. Meng, ACS Nano **7**, 10780 (2013).
[144]Y. S. Kou, S. T. Yang, S. Thiyagu, C. T. Liu, J. W. Wu, and C. F. Lin, Nanoscale **8**(9), 5379 (2016).
[145]Y. T. Lee, F. R. Lin, C. H. Chen, and Z. Pei, ACS Appl. Mater. Interfaces **8**(50), 34537 (2016).
[146]X. Wang, Z. Liu, Z. Yang, J. He, X. Yang, T. Yu, P. Gao, and J. Ye, Small **14**(15), 1704493 (2018).
[147]T. Subramani, H. J. Syu, C. T. Liu, C. C. Hsueh, S. T. Yang, and C. F. Lin, ACS Appl. Mater. Interfaces **8**(3), 2406 (2016).
[148]J. He, P. Gao, Z. Yang, J. Yu, W. Yu, Y. Zhang, J. Sheng, J. Ye, J. C. Amine, and Y. Cui, Adv. Mater. **29**(15), 1606321 (2017).
[149]A. M. Nardes, M. Kemerink, R. A. J. Janssen, J. A. M. Bastiaansen, N. M. M. Kiggen, B. M. W. Langeveld, A. J. J. M. van Breemen, and M. M. de Kok, Adv. Mater. **19**(9), 1196 (2007).
[150]Z. Xia, P. Gao, T. Sun, H. Wu, Y. Tan, T. Song, S. T. Lee, and B. Sun, ACS Appl. Mater. Interfaces **10**(16), 13767 (2018).
[151]J. He, Y. Wan, P. Gao, J. Tang, and J. Ye, Adv. Funct. Mater. **28**(34), 1802192 (2018).
[152]Y. Zhu, T. Song, F. Zhang, S.-T. Lee, and B. Sun, Appl. Phys. Lett. **102**(11), 113504 (2013).
[153]J. He, P. Gao, Z. Ling, L. Ding, Z. Yang, J. Ye, and Y. Cui, ACS Nano **10**(12), 11525 (2016).
[154]Y. Wan, C. Samundsett, J. Bullock, M. Hettick, T. Allen, D. Yan, J. Peng, Y. Wu, J. Cui, A. Javey, and A. Cuevas, Adv. Energy Mater. **7**(5), 1601863 (2017).
[155]Z. Wang, Y. Yang, L. Zhang, H. Lin, Z. Zhang, D. Wang, S. Peng, D. He, J. Ye, and P. Gao, Nano Energy **54**, 99 (2018).
[156]L. Chen, Z. Gao, Y. Zheng, M. Cui, H. Yan, D. Wei, S. Dou, J. Ji, E. Jia, N. Sang, K. Liu, X. Ding, Y. Li, and M. Li, Sol. Energy **174**, 549 (2018).
[157]Y. Zhang, R. Liu, S.-T. Lee, and B. Sun, Appl. Phys. Lett. **104**(8), 083514 (2014).
[158]J. Bullock, P. Zheng, Q. Jeangros, M. Tosun, M. Hettick, C. M. Sutter-Fella, Y. Wan, T. Allen, D. Yan, D. Macdonald, S. De Wolf, A. Hessler-Wyser, A. Cuevas, and A. Javey, Adv. Energy Mater. **6**(14), 1600241 (2016).
[159]Y. Wan, C. Samundsett, J. Bullock, T. Allen, M. Hettick, D. Yan, P. Zheng, X. Zhang, J. Cui, J. McKeon, A. Javey, and A. Cuevas, ACS Appl. Mater. Interfaces **8**(23), 14671 (2016).
[160]J. Sheng, D. Wang, S. Wu, X. Yang, L. Ding, J. Zhu, J. Fang, P. Gao, and J. Ye, RSC Adv. **6**(19), 16010 (2016).
[161]J. Liu, Y. Ji, Y. Liu, Z. Xia, Y. Han, Y. Li, and B. Sun, Adv. Energy Mater. **7**(19), 1700311 (2017).
[162]Y. Han, Y. Liu, J. Yuan, H. Dong, Y. Li, W. Ma, S. T. Lee, and B. Sun, ACS Nano **11**(7), 7215 (2017).
[163]J. He, W. Zhang, J. Ye, and P. Gao, Nano Energy **43**, 117 (2018).
[164]Z. Xia, P. Li, Y. Liu, T. Song, Q. Bao, S.-T. Lee, and B. Sun, Nano Res. **10**(11), 3848 (2017).
[165]Y. Zhang, F. Zu, S.-T. Lee, L. Liao, N. Zhao, and B. Sun, Adv. Energy Mater. **4**(2), 1300923 (2014).
[166]Y. Zhang, W. Cui, Y. Zhu, F. Zu, L. Liao, S.-T. Lee, and B. Sun, Energy Environ. Sci. **8**(1), 297 (2015).
[167]Y. Liu, Z. G. Zhang, Z. Xia, J. Zhang, Y. Liu, F. Liang, Y. Li, T. Song, X. Yu, S. T. Lee, and B. Sun, ACS Nano **10**(1), 704 (2016).
[168]X. Zhang, D. Yang, Z. Yang, X. Guo, B. Liu, X. Ren, and S. F. Liu, Sci. Rep. **6**, 35091 (2016).
[169]D. Zielke, A. Pazidis, F. Werner, and J. Schmidt, Sol. Energy Mater. Sol. Cells **131**, 110 (2014).